Emergent ferromagnetism and *T*-linear scattering in USb_2 at high pressure

Jason R. Jeffries,[1] Ryan L. Stillwell,[1] Samuel T. Weir,[1] Yogesh K. Vohra,[2] and Nicholas P. Butch[3]
[1]*Lawrence Livermore National Laboratory, Livermore, California 94550, USA*
[2]*Department of Physics, University of Alabama at Birmingham, Birmingham, Alabama 35924, USA*
[3]*NIST Center for Neutron Research, National Institute of Standards and Technology, Gaithersburg, Maryland 20899, USA*
(Received 10 February 2016; revised manuscript received 26 April 2016; published 9 May 2016)

The material USb_2 is a correlated, moderately heavy-electron compound within the uranium dipnictide (UX_2) series. It is antiferromagnetic with a relatively high transition temperature $T_N = 204$ K and a large U-U separation. While the uranium atoms in the lighter dipnictides are considered to be localized, those of USb_2 exhibit hybridization and itineracy, promoting uncertainty as to the continuity of the magnetic order within the UX_2. We have explored the evolution of the magnetic order by employing magnetotransport measurements as a function of pressure and temperature. We find that the T_N in USb_2 is enhanced, moving towards that of its smaller sibling UAs_2. But, long before reaching a T_N as high as UAs_2, the antiferromagnetism of USb_2 is abruptly destroyed in favor of another magnetic ground state. We identify this pressure-induced ground state as being ferromagnetic based on the appearance of a strong anomalous Hall effect in the transverse resistance in magnetic field. With pressure, this emergent ferromagnetic state is suppressed and ultimately destroyed in favor of a non-Fermi-liquid ground state.

DOI: 10.1103/PhysRevB.93.184406

I. INTRODUCTION

The famous Hill plot for uranium compounds draws an empirical crossover between magnetic and non-magnetic behavior at a U-U separation of 3.5 Å, the so-called Hill limit [1]. The initial description of the Hill limit assumed that 5f electrons would hybridize *only* with each other; thus, below the Hill limit hybridization would lead to 5f itineracy and above the Hill limit the reduction in hybridization with increasing U-U separation would lead to 5f localization [2]. While this early description does not resonate with modern band structure theory, the Hill limit still offers a respectable degree of predictability for uranium compounds. Binary compounds within the uranium chalcogenides and pnictides exhibit U-U separations ranging from 3.5 up to about 4.5 Å, and generally follow the scenario outlined by Hill, ordering magnetically. Of these compounds, the uranium dipnictides exhibit some of the highest magnetic transition temperatures as well as the largest U-U separations.

While the uranium monopnictides (UX) form in a rock-salt (cubic) structure, the uranium dipnictides (UX_2)—with the exception of UN_2, which forms in the fluorite-type structure—crystallize in a tetragonal structure, the anti-Cu_2Sb prototype. This structure is composed of basal-plane pnictogen layers separated along the c axis by two intervening, corrugated U-X layers. Because the corrugated layers are offset laterally from one another by half of a unit cell, the U ion resides in a ninefold coordinated environment that has three different U-X bond lengths. The tetragonal lattice parameters increase linearly with increasing pnictogen size, but the c/a ratio of the unit cell remains relatively constant just above 2.0.

For phosphorous and larger, the UX_2 compounds order antiferromagnetically, where the U moments are aligned within the basal plane of the U-X layers and antialigned between adjacent corrugated layers (i.e., layers not separated by a pnictogen layer). For X = P, As, and Sb, the spin orientation along the c axis is up/down/down/up, while for X = Bi the orientation is up/down/up/down [3,4]. A crystal-field model with a local tetravalent U ion can at least partly describe the ordered state of the UX_2 series, but the agreement becomes tenuous for USb_2 and was not checked against UBi_2 [5]. Although the unit cell evolves monotonically with increasing pnictogen size, the magnetism of the UX_2 systems reveals a different response. With increasing pnictogen size, the antiferromagnetic (AFM) ordering temperature T_N increases from 203 K for UP_2 up to 273 K for UAs_2. Substitutional studies show that the ordering temperature is a monotonic function of U-U separation for $U(P,As)_2$ [6], but this trend clearly does not extend to USb_2 and UBi_2. For the larger pnictogens, T_N decreases as the U-U separation increases yielding $T_N = 204$ and 183 K for USb_2 and UBi_2, respectively, and suggesting that a strictly local interpretation of the U ion may not be applicable for these larger pnictogens, a trend that is at odds with the simple expectations from the Hill-limit picture.

Both USb_2 and UBi_2 have strong two-dimensional electronic character. Single crystals of USb_2 and UBi_2 exhibit large anisotropies in the resistivity and thermopower depending on whether the measurement is along the a axis or the c axis [7]. These anisotropies manifest from the underlying electronic structure, which comprises cylindrical Fermi surface sheets [8]. De Haas-van Alphen measurements indicate electron masses as high as 6 and 9 m_0 (where m_0 is the mass of a bare electron) for USb_2 and UBi_2, respectively. These enhanced electron masses are consistent with specific heat measurements showing a Sommerfeld coefficient $\gamma \approx 20$ mJ/mol-K^2, suggesting that the U 5f electrons display some itinerant character [9]. Furthermore, angle-resolved photoemission studies of USb_2 reveal a kink in a narrow, dispersing band just below the Fermi level, and Mossbauer spectroscopy proposes a correlation between the hyperfine constant and the effective mass, both promoting the idea of U 5f-electron hybridization with the other conduction electrons [10,11].

Despite its larger lattice parameter and U-U separation, it appears that USb_2 exhibits more hybridization and itineracy of the U 5f-electrons than do the lighter uranium dipnictides.

 ©2016 American Physical Society

Though its 5f electrons show "dual character," the dependence of T_N on U-U separation appears to generally extrapolate towards the more local system UAs_2. While T_N for USb_2 is lower than that of UAs_2, high-pressure studies (< 0.3 GPa) on USb_2 show that its T_N moves upwards with pressure towards that of UAs_2 [12]; however, this observation has not been tested to higher pressures. USb_2 presents an opportunity to explore how hybridization affects the magnetic ordering temperature within the UX_2 series. To that end, we have performed high-pressure electrical transport measurements to interrogate the magnetic ordering in USb_2. Surprisingly, we find that the AFM transition in USb_2 cannot be enhanced to that of UAs_2 due to the abrupt destruction of the AFM state in favor of a new, pressure-induced magnetic ground state.

II. EXPERIMENTAL METHODS

Single crystals of USb_2 were grown via self flux with excess Sb using a U:Sb ratio of 1:6. Depleted U (3N7, New Brunswick Laboratories) and Sb (4N, ESPI Metals) were combined in an alumina crucible, which was sealed in a quartz tube under a partial pressure of UHP Ar. The materials were heated to 1100 °C and held for 96 hours, then slow-cooled to 800 °C over 100 hours, after which the excess flux was spun off in a centrifuge. The crystals formed as platelets up to about 5 mm on a side. Powder and Laue x-ray diffraction were used to confirm the crystal structure [5,13] and single-crystal nature of the samples.

Electrical transport measurements under pressure were performed using a beryllium-copper designer diamond anvil cell (DAC) loaded with solid steatite as a pressure-transmitting medium. A standard diamond anvil (300-μm culet) was paired with a 270-μm-culet, 8-probe designer diamond anvil with tungsten contact pads lithographically deposited onto the exposed microprobes [14–16]. A nonmagnetic MP35N gasket was preindented to a thickness of 40 μm and a 130-μm hole was drilled in the center of the indentation by means of an electric discharge machine (EDM). A small, thin crystallite (approximately $50 \times 50 \times 10$ μm) was placed on the culet of the designer diamond anvil in contact with the tungsten contact pads. Given the planar, tetragonal crystal structure of USb_2, the orientation of the sample was likely to be one in which the larger dimensions represented the basal plane, while the shorter dimension corresponded closer to the c axis.

Pressure was calibrated using the shift in the R1 fluorescence line of ruby [17,18]. Multiple rubies were loaded into the sample chamber, and these rubies were positioned near the sample, but special care was taken to prevent the rubies from bridging between the sample, diamond, or gasket. The sample pressure was calculated as the average of the pressures determined from each ruby, but the multiple rubies also permitted a measurement of the pressure gradients across the sample. The maximum pressure gradient (as a percentage) was 7% at 23.4 GPa, whereas the maximum pressure gradient (in absolute units of pressure) was 1.8 GPa at the highest pressure of 38.0 GPa (less than 5%). The average pressure gradient for all measurements was about 3%. Temperature- and field-dependent, electrical resistance measurements were performed in a commercial cryostat. An antisymmetrization technique was employed to extract the transverse resistance in magnetic field [19].

III. RESULTS AND DISCUSSION

A. Zero-field electrical transport

The temperature-dependent electrical resistivity ρ of USb_2 at selected pressures is shown in Fig. 1; as a comparison, the ambient-pressure data of Wawryk with current along the a axis are included in Fig. 1 [7]. At ambient pressure, ρ exhibits a weak temperature dependence with cooling below 300 K, followed by a dramatic reduction in ρ below $T_N = 202$ K, which signifies the onset of AFM order. On the contrary, Wawryk has shown that the c-axis transport at ambient pressure exhibits an increasing ρ as a sample is cooled below T_N. At the lowest measured pressure of 3.7 GPa, ρ appears to echo the behavior observed at ambient pressure: a weak increase in ρ with decreasing temperature and an abrupt reduction in ρ at T_N. The temperature dependence is consistent with the excepted orientation of the sample within the DAC chamber, which should produce behavior more in line with a-axis transport. The characteristic temperature dependence of USb_2 persists up to 8.3 GPa, showing a continual increase in T_N. However, at 8.3 GPa, a second transition (denoted as T_0) is visible at lower temperature, and this second transition becomes the only one observed for $P \geqslant 9.8$ GPa. The weak temperature dependence of $\rho(T)$ at high temperatures ($T > T_0$ or $T > T_N$) slowly evolves with pressure, ultimately yielding a slightly increasing ρ with increasing T.

Figure 2 displays the numerical derivative of ρ with respect to temperature. The reduction in ρ upon entering the AFM state generates a strong upturn in $d\rho/dT$, and T_N can be readily defined by this feature (see Appendix). With increasing pressure, T_N increases, and the second transition T_0 can be easily identified at $P = 8.3$ GPa. At 9.8 GPa, there is a slight upturn in $d\rho/dT$ near 240 K. This feature is very small, but could indicate that a small fraction of the AFM state remains at these pressures, suggesting that there could be a relatively

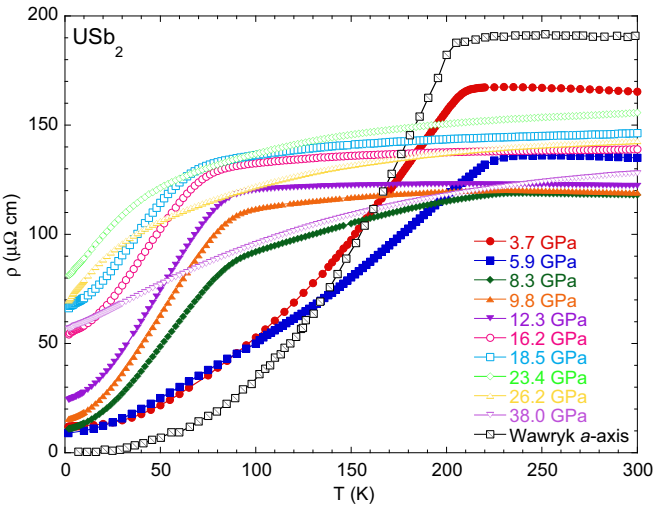

FIG. 1. Electrical resistivity ρ at zero field as a function of temperature T for selected pressures. The data of Wawryk for current along the a axis are from Ref. [7].

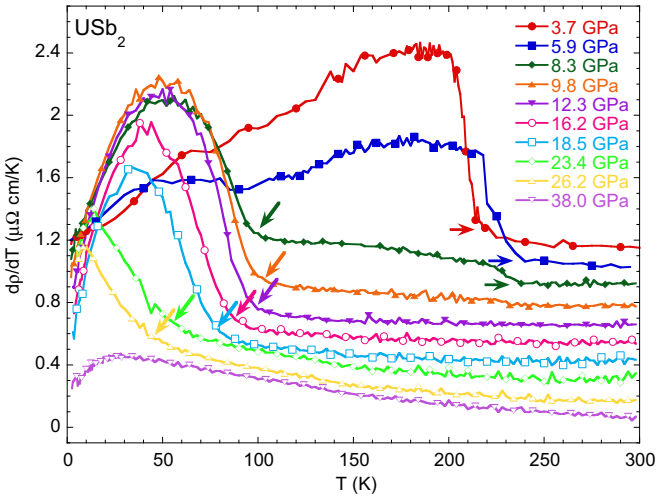

FIG. 2. The derivative of the electrical resistivity $d\rho/dT$ at zero field as a function of T for selected pressures. Right-pointing arrows indicate T_N, while left-pointing (angled) arrows indicate the onset of a new, pressure-induced ordered state at T_0.

broad coexistence region for T_N and T_0. For pressures above 10 GPa, only T_0 is observed in $d\rho/dT$, and T_0 is suppressed with increasing pressure, becoming ill-defined at the highest measured pressures.

B. The pressure-induced ordered state

Simply from the temperature dependence of $\rho(T)$, the nature of the pressure-induced ordered state is not clear, so we turn to magnetotransport measurements to glean insight into the ordered state above $P = 9.8$ GPa and below T_0. Figure 3 shows $\rho(T)$ at 13.8 GPa (where only the transition at T_0 is evident) in various magnetic fields H up to 150 kOe. There is little change in the resistivity curves as a function of applied field. In fact, the main variation in T_0 versus H is correlated to the direction of the temperature sweep (up or down) between field set points. The robustness of T_0 with field may at first suggest ferromagnetic order, but it is not uncommon to have uranium-based AFM systems that exhibit little field dependence up to 150 kOe [20,21].

The transverse resistance (R_{xy}) of USb_2 in magnetic field reveals distinct differences between the AFM state and the pressure-induced ordered state. Example measurements of R_{xy} at 3.7 and 12.3 GPa are shown in Fig. 4. In the AFM state (3.7 GPa), R_{xy} exhibits the linear behavior expected from the conventional Hall effect. Above T_N, R_{xy} shows a positive slope, but R_{xy} exhibits a negative slope below T_N, implying a change in the electronic structure upon entering the AFM state. The onset of AFM order in USb_2 has been shown to cause a Fermi surface reconstruction and enhanced "quasi-two-dimensionality" [9], which is entirely consistent with the sign change observed in the Hall channel of the magneto-transport. At ambient conditions, USb_2 is best described as a compensated electron-hole system [9], so extracting a single carrier density from the linear dependence of R_{xy} seen in Fig. 4(a) would yield a poor description of the system. Assuming a sample thickness of 10 μm permits a definition of R_H, the Hall coefficient, which varies with temperature from 2×10^{-3} to -7×10^{-4} cm^3/C at 3.7 GPa. At higher pressure [Fig. 4(b)], R_{xy} no longer exhibits the characteristic change in sign associated with the onset of AFM order, again highlighting the fact that pressure induces a new, distinct ordered state. Instead, below T_0, R_{xy} deviates from linearity at higher fields, as emphasized by the solid data points at 10, 20, and 50 K plotted in Fig. 4(b).

Deviations from linearity in $R_{xy}(H)$ occur in ferromagnetic (FM) systems and can be accounted for by including an anomalous Hall effect term in the expression for R_{xy}:

$$R_{xy} = R_H H + R_{AHE} = R_H H + R_S M \qquad (1)$$

where $R_H H$ represents the conventional Hall effect, and additional nonlinear field dependence is described by the anomalous Hall component R_{AHE}—which is itself a function

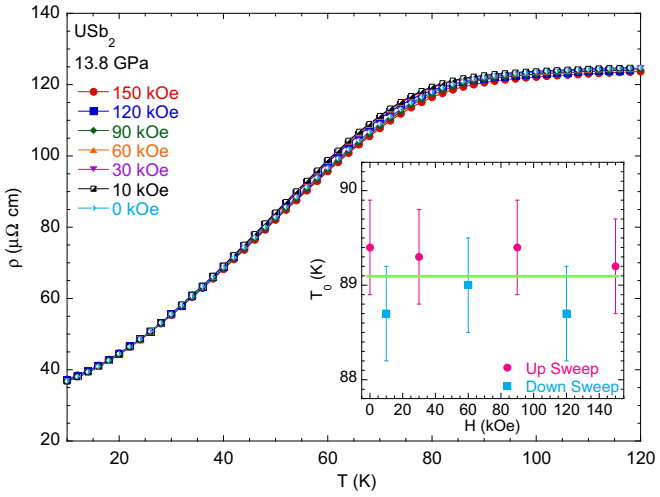

FIG. 3. $\rho(T)$ at 13.8 GPa for various applied fields up to 15 T. The inset shows the value of T_0 as a function of field, differentiating the up and down temperature sweep directions. Error bars are 0.5 K.

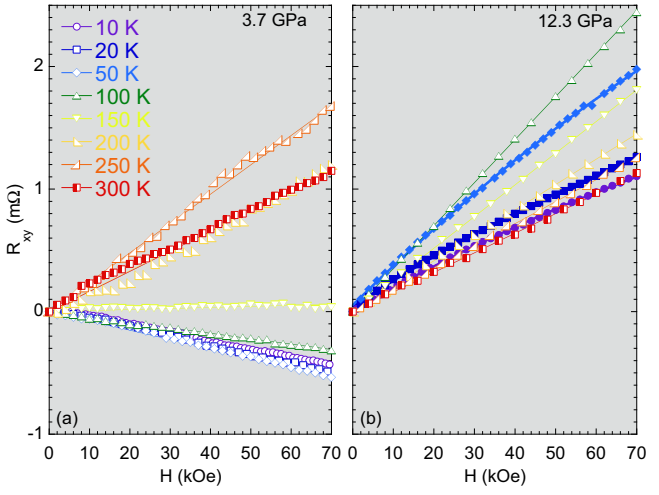

FIG. 4. Transverse resistance R_{xy} versus magnetic field H at fixed temperatures at (a) 3.7 GPa and (b) 12.3 GPa. Thin lines are linear fits to the data, whereas thick lines—10, 20, and 50 K (solid data points) in panel (b)—are interpolations highlighting the curvature in R_{xy}.

of R_S, a scattering coefficient, and M, the magnetization of the system [22]. The anomalous component of R_{xy} can be extracted by fitting the high-field region of R_{xy} with a line ($R_H H$), and subtracting that linear fit from the data to yield $R_{AHE} = R_{xy} - R_H H$ [23]. Example results of this procedure are shown in Fig. 5(a), which plots R_{AHE} versus magnetic field for various temperatures at 14.0 GPa. The resulting R_{AHE} strongly resembles the first quadrant of an archetypal hysteresis loop [$M(H)$] for a FM material, showing a rise with increasing field followed by a saturation above approximately 30 kOe.

We define the saturation value of R_{AHE} as R_M, which we obtain by finding the average value of the data from 30–70 kOe; the error in R_M is defined as the standard deviation in the data from 30–70 kOe. This R_M should be related to the saturation magnetization M_s through the proportionality with R_S dictated from Eq. (1). As a scattering coefficient, R_S can be controlled by several magnetic scattering mechanisms, making quantitative extraction of M_s very challenging [22]. However, the temperature dependence of R_M can be examined as a proxy for M_s. Figure 5(b) shows R_M as a function of temperature along with the expectations for magnetization with mean-field and Ising-type order parameters (for comparison), as well as an order-parameter fit with the critical exponent β as a free parameter:

$$R_M = R_0(1 - T/T_C)^{\beta} \tag{2}$$

where R_0 is simply the zero-temperature limit of R_M and T_C is the critical temperature. The rise in the measured R_M below T_0 is sluggish compared to the two conventional behaviors for magnetization (i.e., mean-field and Ising), but whether this is a true reflection of the pressure-induced magnetic state or an artifact of the unknown temperature dependence of the R_S component of the anomalous Hall effect is difficult to ascertain. The resulting best fit of the data yields $\beta = 1.5 \pm 0.2$ and $T_C = 89 \pm 3$ K; for comparison, $T_0(14.0\ \text{GPa}) = 89.5$ K defined from $\mathrm{d}\rho/\mathrm{d}T$ above. While the critical exponent from this fit may not tell the entire story of the ordered state, it appears that R_M behaves very much like a FM order parameter, implying that the pressure-induced ordered state in USb_2 is FM in nature. At ambient pressure, a conclusion of a FM ground state might be substantiated by magnetization, neutron diffraction, or x-ray magnetic circular dichroism (XMCD). However, at these high pressures near 10 GPa, all of these measurements are challenging, suffering from high backgrounds and small signal. XMCD can be performed in the hard x-ray edge regimes that are amenable to measurements within a DAC at these pressures [24], but the resulting signal is not a direct measure of the magnetic moment, because the magneto-optical sum rules are not valid at these edges [25,26]. As such, these magnetotransport measurements present a picture of the emergent, high-pressure behavior of USb_2 that is very difficult to obtain even with other experimental methods.

The pressure dependence of R_{AHE} can be used to track the evolution of the FM state with pressure. Figure 6(a) shows R_{AHE} at 10 K for pressures between 12.3 and 30.7 GPa. Like before, R_M can be defined, and Fig. 6(b) shows the evolution of R_M versus pressure. After the onset of FM order with pressure, R_M increases to a maximum near 16 GPa, followed by a monotonic decrease until its abrupt disappearance between 28.8 and 30.7 GPa. It is important to note that there is no anomalous Hall component to R_{xy} at 30.7 GPa.

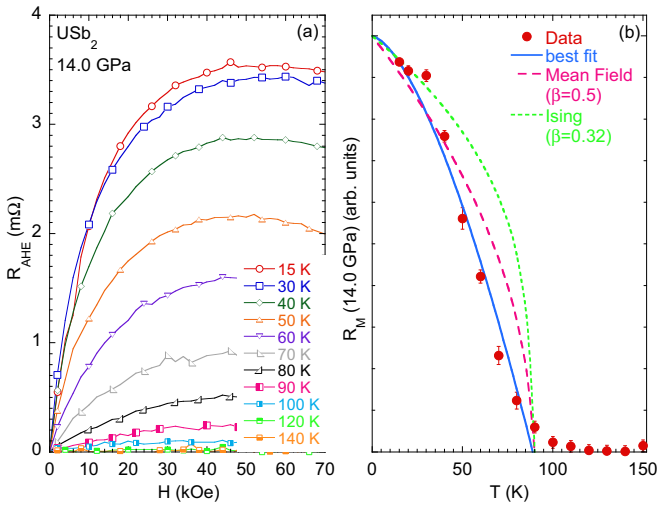

FIG. 5. (a) The anomalous Hall component of R_{xy} (R_{AHE}) at 14.0 GPa versus magnetic field for various temperatures, showing the development of an anomalous Hall signature upon cooling below about 100 K. Lines interpolate between data points. (b) R_M(14.0 GPa), the saturation value of R_{AHE} (see text), as a function of temperature. The solid line is a fit to an order-parameter formula: $\beta = 1.5 \pm 0.2$, whereas the pink and green dashed lines represent the expectations from mean-field and Ising order parameters, respectively. Error bars on the data points represent the standard deviation associated with the definition of R_M (see text).

C. The electronic pressure-temperature phase diagram

A phase diagram from the electrical transport data is shown in Fig. 7, where the characteristic temperatures T_N and T_0 are overlaid upon a contour plot showing the local power-law exponent n determined from the logarithmic derivative of

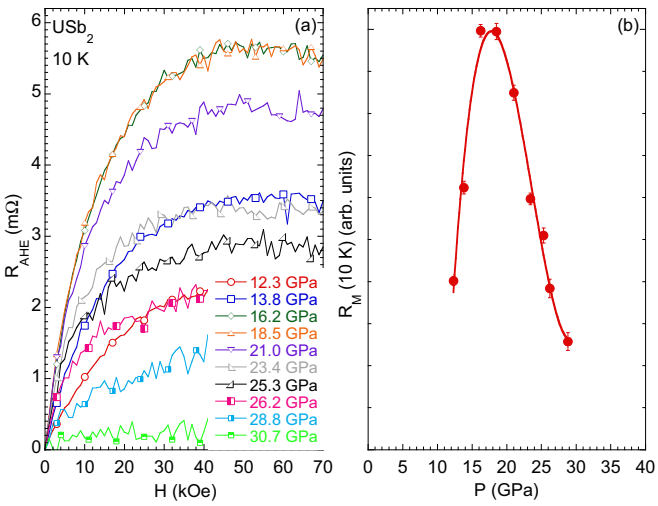

FIG. 6. (a) R_{AHE} versus H measured at 10 K for various pressures; lines interpolate between data points. (b) The evolution of R_M(10 K) versus pressure P. Error bars represent the standard deviation of R_M (see text).

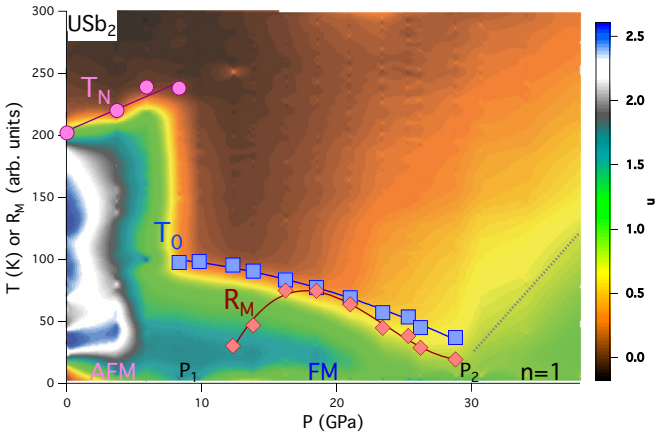

FIG. 7. The electronic phase diagram of USb_2. T_N and T_0 are plotted as purple circles and blue squares, respectively, while R_M(10 K) [arb. units from Fig. 6(b)] is included as red diamonds. Lines between data points are guides to the eye. The contour plot displays n, the local power-law exponent of ρ. The labels P_1 and P_2 mark the approximate locations for the destruction of the AFM state and the pressure-induced FM state, respectively. The high-pressure, T-linear scattering region is demarcated by the dotted, gray line.

$\rho(T)$. The AFM ordering temperature T_N can be seen to increase rapidly with pressure at a rate of about 4.7 K/GPa, about 30% higher than earlier estimates from data limited to 0.3 GPa [12]. The value of T_N only reaches to about 240 K—about half way to that of UAs_2—before disappearing. The disappearance of T_N in favor of T_0 is starkly evident at $P_1 \approx 9$ GPa. T_0 is monotonically suppressed with increasing pressure, and T_0 is no longer evident for pressures above $P_2 \approx 30$ GPa. In addition to a lack of evidence for T_0 in $\rho(T)$, there is a *conspicuous absence* of an anomalous Hall component of R_{xy} for pressures above P_2. This means that the ferromagnetism is abruptly destroyed, falling within a 2-GPa window from a nonzero R_M with $T_0 = 35$ K at 28.8 GPa to a completely nonmagnetic ground state above P_2. This abrupt, first-order-like destruction of long-range order is a common feature of ferromagnets driven towards a quantum phase transition [27–29]. In addition to T_N and T_0, the phase diagram of Fig. 7 contains the 10-K value of R_M from Fig. 6 b (plotted in arbitrary units along the vertical axis) to compare the pressure dependence of R_M with that of T_0. For $P > 16$ GPa, the pressure dependencies of R_M and T_0 track reasonably well, but for $12 < P < 16$ GPa, R_M rises while T_0 decreases. This opposing pressure dependence just above P_1 could be due to inhomogeneities in the FM state associated with the transition away from AFM order.

For pressures below P_1 and at high temperatures, n is small owing to the weak temperature dependence characteristic of heavy fermion materials [30]. This weak temperature dependence at high temperatures (above the ordering transitions) evolves slightly with pressure, but, even at the highest pressures, n remains sub-linear near room temperature. Below T_N, $n = 2.5$ at ambient pressure [7], but n is driven to lower values with increasing pressure. For $P > P_1$, in the FM state, ρ varies nearly as $T^{3/2}$ for temperatures up to about $0.7{*}T_0$, and this behavior persists up to about 20 GPa. Between 20 GPa and P_2, ρ shows a nearly linear temperature dependence below T_0. Above P_2, there is an expanding region where $n = 1$ that emanates from P_2 and extends in excess of 100 K at 38 GPa, behavior that is often classified as non-Fermi liquid (NFL) behavior and often associated with quantum criticality [31–33]. Near the destruction of the FM phase, the measured residual resistivity is large, accounting for the majority of the total resistivity observed at the high-temperature boundary of the T-linear scattering region. The high residual resistivity may indicate phase inhomogeneity, which can make interpretation of the temperature dependence challenging. Neither superconductivity nor normal-state Fermi-liquid behavior are observed above 2 K in USb_2.

Several U-based ferromagnets (e.g., UGe_2, URhAl, UCoAl, etc.) show pressure-driven features similar to that of the FM portion of the USb_2 phase diagram: namely the abrupt destruction of the FM state and the development of NFL behavior [29]. These U-based systems have, thus far, been tuned by moderate pressures, typically below 5 GPa. Often in concert with the disappearance of ferromagnetism in these systems is the development of "tri-critical wings" in a pressure-temperature-field (P-T-H) phase diagram [27–29,34]. The observation of NFL behavior is typically confined to a small region of phase space within these wings. Measurements potentially providing evidence for tri-critical wings near P_2 in USb_2 were not performed. However, the NFL-like behavior of USb_2 spans a very large range in temperature that exceeds even the ordering temperature below P_2, suggesting that the criticality and NFL-like behavior that arise above P_2 in USb_2 may be different from other U-based ferromagnets. Indeed, the size of the T-linear scattering region in USb_2 is more reminiscent of the cuprate materials than typical heavy fermion systems. However, the T-linear scattering in the cuprates is associated with AFM fluctuations [35–38], whereas the NFL-like behavior of USb_2 arises near a FM phase boundary, a conundrum that may suggest that AFM fluctuations reside within the FM state of USb_2. Another scenario proposed for quantum critical ferromagnets is the development of other intermediate phases near the destruction of ferromagnetism [39]. Such a scenario in USb_2 at high pressure could give rise to additional magnetic fluctuations that drive the observed T-linear scattering.

IV. CONCLUSIONS

High pressure has a strong effect on the magnetism of USb_2, enhancing T_N at a rate of 4.7 GPa/K and yielding a $T_N = 240$ K at 8.3 GPa, about halfway to the highest values in the UX_2 series of 273 K in UAs_2. However, for $P > P_1$ the antiferromagnetism of USb_2 is destroyed, and a new magnetic ground state emerges with a $T_0 = 98$ K. This high-pressure magnetic ground state is ferromagnetic, as determined from the presence of an anomalous Hall component in the transverse resistance in magnetic field. The magnitude of this anomalous Hall component (R_M) appears to be a good proxy for the magnetization of the material, and R_M increases to a maximum near 16 GPa, where $T_0 = 84$ K. For pressures in excess of 16 GPa, both the FM transition temperature and R_M are suppressed, and, near $P_2 \approx 30$ GPa, both discontinuously disappear in a manner similar to other FM quantum critical

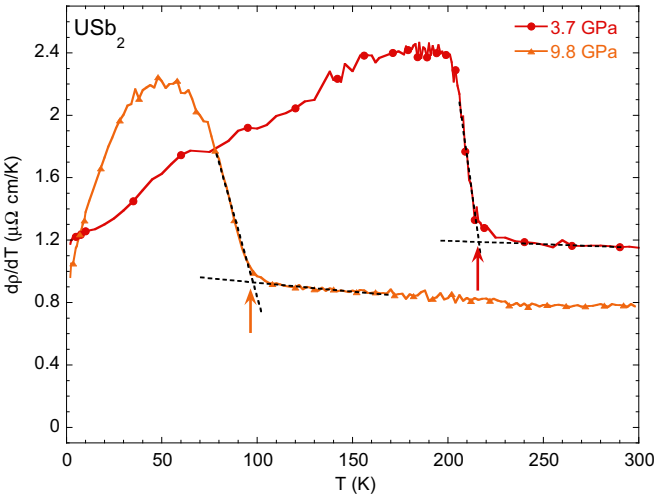

FIG. 8. T_N and T_0 were defined from a "knee temperature" construction. Extrapolations of the temperature dependence above and below the transitions are shown as dotted lines. The intersection of these extrapolated lines are denoted by the upward pointing arrows.

systems. At these high pressures where ferromagnetism has been suppressed, the electrical resistivity exhibits a region of NFL-like, T-linear scattering that emanates from P_2, perhaps suggesting a broad region where quantum critical fluctuations dominate the material. The mechanism driving this T-linear behavior is currently unknown, and it does not appear to be completely analogous to other cuprate or heavy fermion systems, perhaps suggesting a novel origin.

ACKNOWLEDGMENTS

We thank G. Lander, P. Söderlind, and J. Paglione for valuable comments and discussion. We are very grateful to S. K. McCall and J. R. I. Lee for their assistance with maintaining/operating the cryostat. This work was supported by LDRD (Tracking Code 14-ERD-041) at Lawrence Livermore National Laboratory. Lawrence Livermore National Laboratory is operated by Lawrence Livermore National Security, LLC, for the US Department of Energy, National Nuclear Security Administration under Contract DE-AC52-07NA27344. Y.K.V. acknowledges support from DOE-NNSA Grant No. DE-NA0002014.

APPENDIX:

CHARACTERISTIC TEMPERATURES FROM $d\rho/dT$

The characteristic temperatures T_N and T_0 for the ordered phases observed from electrical transport were defined from the following "knee temperature" construction: Data above and below the transition observed in $d\rho/dT$ were linearly extrapolated, and the intersection of those extrapolations was used to define T_N or T_0. Examples of this procedure for 3.7 and 9.8 GPa are shown in Fig. 8.

[1] H. H. Hill, in *Plutonium 1970 and other Actinides*, edited by W. H. Miner (Metallurgical Society AIME, New York, 1970), Vol. 17, p. 2.
[2] A. M. Boring and J. S. Smith, Los Alamos Sci. **26**, 90 (2000).
[3] R. Troć, J. Leciejewicz, and R. Ciszewski, Phys. Status Solidi **15**, 515 (1966).
[4] J. Leciejewicz, R. Troć, A. Murasik, and A. Zygmut, Phys. Status Solidi **22**, 517 (1967).
[5] G. Amoretti, A. Blaise, and J. Mulak, J. Magn. Magn. Mater. **42**, 65 (1984).
[6] Z. Henkie, R. Maślaka, P. Wiśniewski, R. Fabrowski, P. J. Markowski, J. J. M. Franse, and M. van Spring, J. Alloys Compd. **181**, 267 (1992).
[7] R. Wawryk, Philos. Mag. **86**, 1775 (2006).
[8] S. Lebègue, P. M. Oppeneer, and O. Eriksson, Phys. Rev. B **73**, 045119 (2006).
[9] D. Aoki, P. Wiśniewski, K. Miyake, N. Watanabe, Y. Inada, R. Settai, E. Yamamoto, Y. Haga, and Y. Onuki, Philos. Mag. B **80**, 1517 (2000).
[10] S. Tsutsui, M. Nakada, S. Nasu, Y. Haga, D. Aoki, P. Wiśniewski, and Y. Onuki, Phys. Rev. B **69**, 054404 (2004).
[11] X. Yang, P. S. Riseborough, T. Durakiewicz, C. G. Olsen, J. J. Joyce, E. D. Bauer, J. L. Sarrao, D. P. Moore, K. S. Graham, S. Elgazzar, P. M. Oppeneer, E. Guziewicz, and M. T. Butterfield, Philos. Mag. **89**, 1893 (2009).
[12] Z. Henkie, P. Wiśniewski, R. Fabrowski, and R. Maślaka, Solid State Commun. **79**, 1025 (1991).
[13] F. Grønvold, M. R. Zaki, E. F. Westrum, Jr., J. A. Sommers, and D. B. Downie, J. Inorg. Nucl. Chem. **40**, 635 (1978).
[14] S. T. Weir, J. Akella, C. Aracne-Ruddle, Y. Vohra, and S. A. Catledge, Appl. Phys. Lett. **77**, 3400 (2000).
[15] J. R. Patterson, S. A. Catledge, Y. K. Vohra, J. Akella, and S. T. Weir, Phys. Rev. Lett. **85**, 5364 (2000).
[16] J. R. Jeffries, N. P. Butch, K. Kirshenbaum, S. R. Saha, G. Samudrala, S. T. Weir, Y. K. Vohra, and J. Paglione, Phys. Rev. B **85**, 184501 (2012).
[17] H. K. Mao, J. Xu, and P. M. Bell, J. Geophys. Res. **91**, 4673 (1986).
[18] W. L. Vos and J. A. Schouten, J. Appl. Phys. **69**, 6744 (1991).
[19] J. R. Jeffries, P. Söderlind, H. Cynn, A. Landa, W. J. Evans, S. T. Weir, Y. K. Vohra, and G. H. Lander, Phys. Rev. B **87**, 214104 (2013).
[20] A. Suslov, J. B. Ketterson, D. G. Hinks, D. F. Agterberg, and B. K. Sarma, Phys. Rev. B **68**, 020406(R) (2003).
[21] A. V. Andreev, S. Yasin, Y. Skourski, A. A. Zvyagin, S. Zherlitsyn, and J. Wosnitza, Phys. Rev. B **87**, 214409 (2013).
[22] N. Nagaosa, J. Sinova, S. Onoda, A. H. MacDonald, and N. P. Ong, Rev. Mod. Phys. **82**, 1539 (2010).
[23] R. L. Stillwell, J. R. Jeffries, S. K. McCall, J. R. I. Lee, S. T. Weir, and Y. K. Vohra, Phys. Rev. B **92**, 174421 (2015).
[24] J. R. Jeffries, L. S. I. Veiga, G. Fabbris, D. Haskel, P. Huang, N. P. Butch, S. K. McCall, K. Holliday, Z. Jenei, Y. Xiao, and P. Chow, Phys. Rev. B **90**, 104408 (2014).

[25] B. T. Thole, P. Carra, F. Sette, and G. van der Laan, Phys. Rev. Lett. **68**, 1943 (1992).
[26] P. Carra, B. T. Thole, M. Altarelli, and X. Wang, Phys. Rev. Lett. **70**, 694 (1993).
[27] V. Taufour, D. Aoki, G. Knebel, and J. Flouquet, Phys. Rev. Lett. **105**, 217201 (2010).
[28] D. Aoki, T. Combier, V. Taufour, T. D. Matsuda, G. Knebel, H. Kotegawa, and J. Flouquet, J. Phys. Soc. Jpn. **80**, 094711 (2011).
[29] M. Brando, D. Belitz, F. M. Grosche, and T. R. Kirkpatrick, arXiv:1502.02898.
[30] G. R. Stewart, Rev. Mod. Phys. **56**, 755 (1984).
[31] G. R. Stewart, Rev. Mod. Phys. **73**, 797 (2001).
[32] P. Coleman and A. J. Schofield, Nature (London) **433**, 226 (2005).
[33] J. Paglione, T. A. Sayles, P.-C. Ho, J. R. Jeffries, and M. B. Maple, Nat. Phys. **3**, 703 (2007).
[34] Y. Shimizu, D. Braithwaite, B. Salce, T. Combier, D. Aoki, E. N. Hering, S. M. Ramos, and J. Flouquet, Phys. Rev. B **91**, 125115 (2015).
[35] A. J. Schofield, Contemp. Phys. **40**, 95 (1999).
[36] T. Das, R. S. Markiewicz, and A. Bansil, Phys. Rev. B **81**, 184515 (2010).
[37] K. Jin, N. P. Butch, K. Kirshenbaum, J. Paglione, and R. L. Greene, Nature (London) **476**, 73 (2011).
[38] N. P. Butch, K. Jin, K. Kirshenbaum, R. L. Greene, and J. Paglione, Proc. Natl. Acad. Sci. **109**, 8440 (2012).
[39] U. Karahasanovic, F. Krüger, and A. G. Green, Phys. Rev. B **85**, 165111 (2012).